

# Control of open quantum systems: Manipulation of a qubit coupled to a thermal bath by an external driving field.

Haoran Sun<sup>1</sup> and Michael Galperin<sup>1,\*</sup>

<sup>1</sup>*Department of Chemistry & Biochemistry, University of California San Diego, La Jolla, CA 92093, USA*

Fast and reliable manipulation with qubits is fundamental for any quantum technology. The implementation of these manipulations in physical systems is the focus of studies involving optimal control theory. Realistic physical devices are open quantum systems. So far, studies in optimal control theory have primarily utilized the Redfield/Lindblad quantum master equation to simulate the dynamics of such systems. However, this Markov description is not always sufficient. Here, we present a study of qubit control utilizing the nonequilibrium Green's function method. We compare the traditional master equation with more general Green's function results and demonstrate that even in the parameter regime suitable for the application of the Redfield/Lindblad approach, the two methods yield drastically different results when addressing evolution involving mixed states. In particular, we find that, in addition to predicting different optimal driving profiles, a more accurate description of system evolution enables the system to reach the desired final state much more quickly. We argue that the primary reason for this is the significance of the non-Markov description of driven system dynamics due to the effect of time-dependent driving on dissipation.

## I. INTRODUCTION

The capability to create, transfer, and read quantum information forms the basis of quantum measurement<sup>1</sup>, quantum metrology<sup>2</sup>, and quantum computing<sup>3,4</sup>. Corresponding methods and limits of information manipulation are explored in research on quantum steering<sup>5</sup>, quantum resource theories<sup>6</sup>, and quantum thermodynamics<sup>7-9</sup>. Notably, the rapid and reliable reset of a qubit is a crucial prerequisite for any quantum technology<sup>10,11</sup>. The implementation of these manipulations in physical systems is the focus of studies in quantum optimal control theory (OCT)<sup>12-17</sup>.

Optimal control addresses the challenge of achieving a desired quantum state of a system in the most efficient manner. Typically, this control is implemented using time-dependent external fields. Initially, optimal control theory concentrated on isolated quantum systems, where the Schrödinger equation governed the system's evolution<sup>18-26</sup>. Effective computational algorithms for attaining the desired outcomes in such systems are documented in the literature<sup>27,28</sup>.

Realistic experimental setups involve open quantum systems. The need to consider the open nature of the system has led to modifications in OCT studies. Initially, a surrogate Hamiltonian approach was proposed<sup>29-33</sup>. In this approach, the Schrödinger equation is applied to a finite surrogate Hamiltonian that substitutes the physical (infinite) system-bath description. This finite representation is crafted to produce reasonable short-time dynamics of the system coupled to an infinite bath.

To simulate longer trajectories and incorporate accurate thermodynamic behavior, the open character of the system should be considered more precisely. This led to the substitution of Schrödinger with the quantum master equation (QME) as the dynamical law in OCT studies. Since optimization relies on an iterative procedure, QME is typically employed in its most basic (Red-

field/Lindblad) form. Following tradition, OCT considerations with QME as the dynamical law overlook the influence of the time-dependent field on the dissipator<sup>34-43</sup>. Subsequently, to enhance modeling realism, the effect of the field on the dissipator was incorporated within the instantaneous (adiabatic) approximation<sup>44,45</sup>.

Markov evolution simulated within the Redfield/Lindblad QME (similar to other weak coupling theories<sup>46</sup>) is not always accurate in predicting open system responses<sup>47,48</sup>. Thus, non-Markov OCT was performed for the spin-boson system using the hierarchical equation of motion approach (HEOM)<sup>49</sup>. HEOM is a highly promising technique for simulating time-dependent and transient processes due to its linear scaling with time. Early versions of HEOM were restricted to high temperatures and specific band structures. Subsequent developments allow for trading some of its advantages for significantly improved access to more general band structures and lower temperatures<sup>50</sup>. Nevertheless, it remains unclear whether experimentally relevant low temperatures are achievable with this technique.

Green's function methods<sup>51</sup> are capable of overcoming the limitations of the techniques used in OCT literature so far. Here, we employ the nonequilibrium Green's function (NEGF) method in OCT studies of a qubit. Following Ref. 45 we consider optimization of laser pulse with goals of heating, cooling, and particular state preparation of an open quantum system. We compared QME results with more general NEGF simulations. We note that there are two aspects to quantum control analysis: 1. the optimal control method and 2. the theoretical approach used to describe the evolution of the system. In our study we follow the optimal control method employed in Ref. 45. While more advanced optimization methods are available in OCT literature, focus of our consideration is description of the evolution of the system. We suggest the NEGF approach exemplified here and<sup>47,48</sup> in non-Markov scenarios of strong driving/coupling, where

the usual Markov (Redfield/Lindblad-type) approaches become inaccurate. In those cases, NEGF could be a way around solving the non-Markov integro-differential equations with memory kernels. Besides preserving complete positivity of the system density operator<sup>52</sup>, NEGF is capable of proper description of system-bath interaction including quantum effects (bath induced coherences) and influence of time-dependent driving on the coupling. In this sense, choice of optimization procedure is of secondary importance.

The structure of the paper is as follows. Section II introduces the model and describes the methods used in the simulations. A comparison between the numerical results of QME and NEGF simulations is presented in Section III. Section IV summarizes our findings.

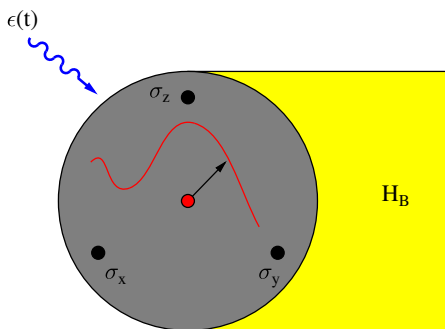


FIG. 1. (Color online) Sketch of a qubit coupled to a thermal bath and driven by external field.

## II. CONTROL OF QUBIT COUPLED TO BATH

Here, we introduce the model, describe the methods employed in the simulations of the system dynamics, and discuss the optimization procedure.

### A. Model

Following Ref. 45 we consider a qubit  $S$  coupled to thermal bath  $B$  and driven by external time-dependent field  $\epsilon(t)$  (see Fig. 1)

$$\hat{H}(t) = \hat{H}_S(t) + \hat{H}_B + \hat{H}_{SB} \quad (1)$$

where  $\hat{H}_S(t)$  and  $\hat{H}_B$  describe decoupled system and bath, respectively.  $\hat{H}_{SB}$  introduces interaction between them. Explicit expressions are (here and below  $\hbar = k_B =$

1)

$$\hat{H}_S(t) = \sum_{i=1}^2 \Delta \hat{n}_i + \frac{\Delta}{2} (\hat{d}_1^\dagger \hat{d}_2 + \text{H.c.}) \quad (2)$$

$$+ \frac{\epsilon(t)}{2} (\hat{n}_2 - \hat{n}_1)$$

$$\hat{H}_B = \sum_{\alpha} \omega_{\alpha} \left( \hat{a}_{\alpha}^{\dagger} \hat{a}_{\alpha} + \frac{1}{2} \right) \quad (3)$$

$$\hat{H}_{SB} = \frac{i}{2} (\hat{d}_2^{\dagger} \hat{d}_1 - \hat{d}_1^{\dagger} \hat{d}_2) \sum_{\alpha} g_{\alpha} (\hat{a}_{\alpha} + \hat{a}_{\alpha}^{\dagger}) \quad (4)$$

Here,  $\hat{d}_i^{\dagger}$  ( $\hat{d}_i$ ) and  $\hat{a}_{\alpha}^{\dagger}$  ( $\hat{a}_{\alpha}$ ) creates (annihilates) electron in level  $i$  ( $i = 1, 2$ ) and excitation in mode  $\alpha$  of thermal bath, respectively.  $\hat{n}_i \equiv \hat{d}_i^{\dagger} \hat{d}_i$  is the particle number operator. Driving field  $\epsilon(t)$  is modeled as set of harmonic modes acting within a finite time interval

$$\epsilon(t) = \exp \left[ - \left( \frac{t - t_c/2}{t_c} \right)^2 \right] \sum_{k=1}^M c_k \sin(\nu_k t) \quad (5)$$

where,  $M$  is the number of harmonic modes in the signal and  $t_c$  is the control time.

Note that the Hamiltonian commutes with the system total particle number operator

$$[\hat{H}(t), \hat{n}_1 + \hat{n}_2] = 0 \quad (6)$$

Thus, the formulation properly describes qubit (spin-1/2) evolution when confined to the one-particle subspace.

### B. QME formulation

Following Ref. 45, for the standard OCT treatment, we simulate the system's evolution using the Redfield/Lindblad QME. We utilize an advanced version of the QME that accounts for the effect of a time-dependent driving field on the dissipation superoperator<sup>53</sup>. The corresponding Markov EOM for the system's density operator in the interaction picture is (see Appendix A for details)

$$\begin{aligned} \frac{d}{dt} \hat{\rho}_S(t) = \sum_m \left\{ -i \text{Im}(\Gamma_m(t)) [\hat{F}_m^{\dagger}(t) \hat{F}_m(t), \hat{\rho}_S(t)] \right. \\ \left. + 2 \text{Re}(\Gamma_m(t)) \left[ \hat{F}_m(t) \hat{\rho}_S(t) \hat{F}_m^{\dagger}(t) \right. \right. \\ \left. \left. - \frac{1}{2} \{ \hat{F}_m^{\dagger}(t) \hat{F}_m(t), \hat{\rho}_S(t) \} \right] \right\} \quad (7) \end{aligned}$$

Here,  $\hat{F}_m(t)$  and  $\Gamma_m(t)$  are the jump operators and time-dependent coefficients defined in Eqs. (A5) and (A13), respectively.

### C. NEGF formulation

Single particle Green's function

$$G_{ij}(\tau_1, \tau_2) = -i \langle T_c d_i(\tau_1) d_j^{\dagger}(\tau_2) \rangle \quad (8)$$

is the central object to describe dynamics of the system within the NEGF. Here,  $\tau_{1,2}$  are the Keldysh contour variables,  $T_c$  is the contour ordering operator, and  $\hat{d}_i^\dagger(\tau)$  ( $\hat{d}_i(\tau)$ ) is the electron creation (annihilation) operator in the Heisenberg picture. Single particle density matrix is given by the lesser projection of the Green's function

$$\rho_{ij}(t) = -i G_{ij}^<(t, t) \quad (9)$$

Within the NEGF, dynamics of the system is governed by the Kadanoff-Baym equation

$$\begin{aligned} i \frac{\partial}{\partial \tau_1} G_{ij}(\tau_1, \tau_2) &= \delta_{i,j} \delta(\tau_1, \tau_2) \\ &+ \sum_m [H_S(t_1)]_{im} G_{mj}(\tau_1, \tau_2) \\ &+ \sum_m \int_c d\tau \Sigma_{im}(\tau_1, \tau) G_{mj}(\tau, \tau_2) \end{aligned} \quad (10)$$

Here,  $t_1$  is physical time corresponding to contour variable  $\tau_1$ .  $\Sigma$  is the self-energy which describes the influence of the bath. Its explicit expression within the Hartree-Fock approximation is given in Eqs. (B4)-(B6).

#### D. Control tasks

Dynamical trajectories generated within QME or NEGF are used in an iterative procedure to reach control tasks. Below we consider three such tasks: reaching a particular quantum state (reset), heating, and cooling of the system.

The tasks are achieved by optimization of the driving force profile  $\epsilon(t)$ . Specifically, we use coefficients  $c_k$  in the Fourier series (5) as adjustable parameters, while frequencies  $\nu_k$  are fixed

$$\nu_k = \frac{k\pi}{t_c}, \quad k = 1, 2, 3, \dots \quad (11)$$

We start with a decoupled qubit and bath with the qubit being in an initial state  $\hat{\rho}_i = \hat{\rho}(t=0)$ . Within a predefined finite control time  $t_c$ , we search for such driving force profile  $\epsilon(t)$  that by the time  $t = t_c$  the qubit evolves to some desired state  $\hat{\rho}_f \approx \hat{\rho}(t_c)$ . Note that the density operator of a qubit can be decomposed as

$$\hat{\rho} = \left( \frac{1}{2} + x \hat{s}_x + y \hat{s}_y + z \hat{s}_z \right) \quad (12)$$

Here,  $\hat{s}_{x,y,z}$  are the spin-1/2 operators. That is, state of the qubit is fully defined by vector  $(x, y, z)$  and can be represented as a point within 3D unit sphere, while distance between two states can be defined as distance between a pair of 3D vectors.

Quality of the control is defined by a cost function  $R[\hat{\rho}_i, \epsilon(t)]$ . That is, goal of the optimization is finding functions  $c_k(t)$  which minimize the cost function. In particular, for reset (r) and heating (h) tasks, the cost function is defined as the distance between the state of the

system at the end of the trajectory,  $\hat{\rho}(t_c)$ , and desired outcome  $\hat{\rho}_f$

$$R_{r,h}[\hat{\rho}_i, \epsilon(t)] \equiv \|\hat{\rho}_f - \hat{\rho}(t_c)\| \quad (13)$$

The cost function for the cooling (c) task is defined as

$$R_c[\hat{\rho}_i, \epsilon(t)] \equiv -\|\hat{\rho}(t_c)\|^2 \quad (14)$$

This form is used because of its faster convergence.

### III. NUMERICAL RESULTS AND DISCUSSION

Time evolution within the QME formulation is numerically simulated using the Runge-Kutta method of fourth order (RK4)<sup>54</sup>. Time propagation within the NEGF formulations is simulated following a scheme introduced in Ref. 55. The NEGF simulations employ Fast Fourier transform (FFT) which is numerically performed utilizing the FFTW library<sup>56</sup>. Differential evolution<sup>57</sup> is employed as an optimization algorithm to find driving force profile for both QME and NEGF dynamics, the same random generator, iterative depth and population size are used in both cases.

Below we compare results of simulations within QME and NEGF for the optimized driving force  $\epsilon(t)$ , entropy production  $S_i(t)$ , entropy  $S(t)$ , and cost function  $R[\hat{\rho}_i, \epsilon(t)]$ . Entropy is obtained by integrating differential form of the second law of thermodynamics

$$\frac{d}{dt} S(t) = \beta \dot{Q}_B(t) + \dot{S}_i(t) \quad \dot{S}_i(t) \geq 0 \quad (15)$$

where  $\dot{Q}_B(t)$  and  $\dot{S}_i(t)$  are heat flux between the qubit and thermal bath and entropy production rate, respectively. Heat flux is defined as rate of energy change in the bath

$$\dot{Q}_B(t) = -\sum_\alpha \omega_\alpha \frac{d}{dt} \langle \hat{a}_\alpha^\dagger(t) \hat{a}_\alpha(t) \rangle \quad (16)$$

Expressions for entropy and entropy production depend on formulation of the second law. For systems weakly coupled to their baths (QME formulation) the former is given by the von Neumann expression

$$S(t) = -\text{Tr}_S \{ \hat{\rho}_S(t) \ln \hat{\rho}_S(t) \} \quad (17)$$

which together with expression for heat flux yields entropy production rate<sup>58</sup>

$$\begin{aligned} \dot{Q}_B(t) &= \text{Tr}_S \{ (\mathcal{L}_D \rho_S(t)) \hat{H}^S(t) \} \\ \dot{S}_i(t) &= -\text{Tr}_S \{ (\mathcal{L}_D \rho_S(t)) \ln \hat{\rho}_S(t) \} \end{aligned} \quad (18)$$

Here,  $\mathcal{L}_D$  is dissipator part of the Liouvillian defined by the last two lines of Eq.(7).

For systems strongly coupled to their baths we follow formulation of Ref. 59. Expressions for heat flux and

entropy production rate are

$$\begin{aligned}\dot{Q}_B(t) &= \int_0^\infty \frac{d\omega}{2\pi} \omega i_B(t, \omega) \\ \dot{S}_i(t) &= \int_0^\infty \frac{d\omega}{2\pi} \left\{ \phi^{out}(t, \omega) [\ln \phi^{out}(t, \omega) - \ln \phi^{in}(\omega)] \right. \\ &\quad \left. - (1 + \phi^{out}(t, \omega)) [\ln(1 + \phi^{out}(t, \omega)) - \ln(1 + \phi^{in}(\omega))] \right\}\end{aligned}\quad (19)$$

Here,  $i_B(t, \omega)$  is the energy resolved particle (phonon) flux between the system and thermal bath defined in Eq. (C9),  $\phi^{in}(\omega)$  and  $\phi^{out}(t, \omega)$  are the thermal population of incoming and non-thermal population of outgoing states in the bath. Explicit expressions for the current and populations in terms of the Green's function (8) are given in Appendix C.

The parameters of the simulations are level separation  $\Delta$ , Eq.(2), dissipation rate  $\gamma_0$  and cut-off frequency of the bath spectral function (see Eqs. (B7)-(B9) for definitions), inverse temperature  $\beta$ , Eq.(B10), driving force number of modes  $M$  and bound on signal amplitude  $\max|c_k|$ , Eq.(5), size and step of the FFT grid, and maximum number of iterations employed by the optimization algorithm. Control time  $t_c$  is defined in each control task. Below, all energies are presented in units of level separation  $\Delta$ , time unit is  $1/\Delta$ . Numerical values of the parameters are collected in Table I. We note that the parameters are favorable for the applicability of the Redfield QME.

TABLE I. Parameters for numerical simulation

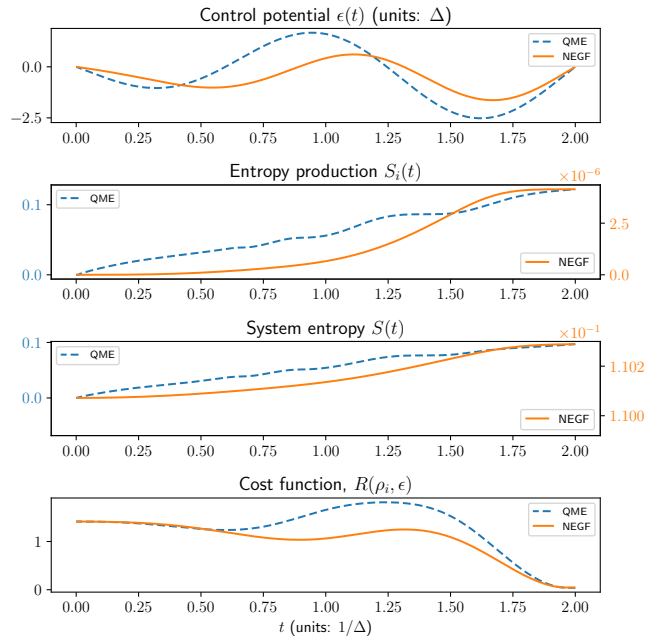
Parameter	Value
$\Delta$	1
$\gamma_0$	0.5
$\omega_c$	5
$\beta^{-1}$	1
$M$	4
$\max c_k $	10
Size of the FFT grid	80000
Energy step of the grid	$\pi/t_c$
Max number of iterations	10
Population size	15

We now present results of simulations within the QME and NEGF for reset, heating, and cooling of qubit.

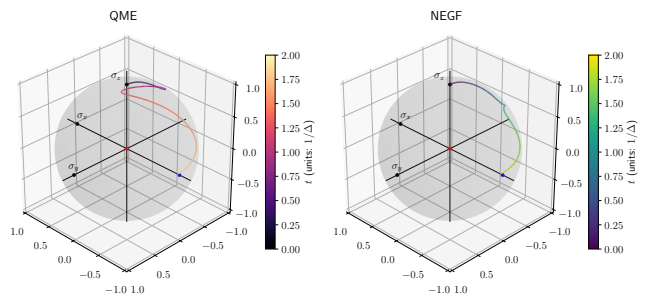
### A. Reset

System starts in an arbitrary pure state and control goal is to bring it to a specific predefined pure state. As an example, we consider system evolution from  $\rho_i = (I + \sigma_z)/2$  to  $\rho_f = (I - \sigma_x)/2$ . Here,  $I$  is the identity matrix.

Figure 2 shows results of simulations performed within QME and NEGF for  $t_c = 2$ . The performance of optimization within the two formulations is very similar.



(a)



(b)

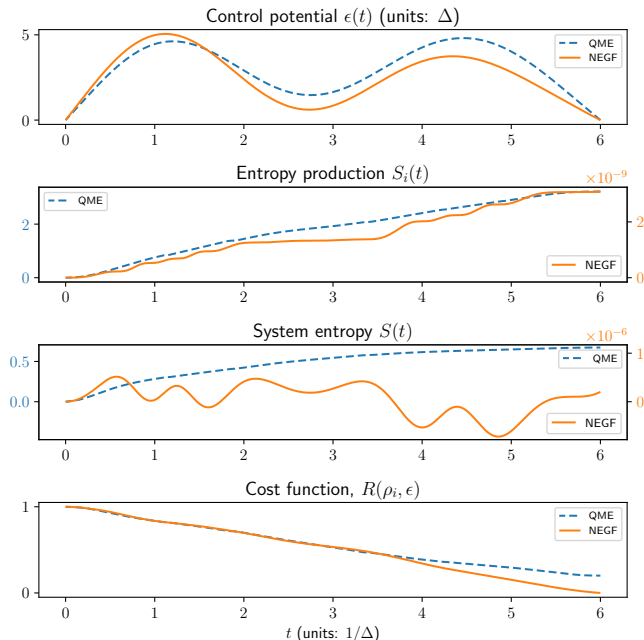
FIG. 2. (Color online) Reset of the qubit: forced evolution from an arbitrary initial state ( $\rho_i = (I + \sigma_z)/2$ ) to a predefined final state ( $\rho_f = (I - \sigma_x)/2$ ). Panel (a) shows (top to bottom) optimal driving force potential, entropy production, entropy of the qubit, and cost function vs. time simulated within QME (dashed line, blue) and NEGF (solid line, orange). Panel (b) shows trajectories of the system within the two formulations.

Qualitative behavior of the qubit response is the same (see panel a) with NEGF results demonstrating a slight time delay - a manifestation of the non-Markov character of the evolution. As expected, entropy production is seen to level by the end of the driving. Both schemes are capable of reaching the control goal with the same accuracy. Note that even trajectories (see panel b) are quite similar in the short time for the two methods. This similarity is observed also in the other control tasks discussed below and is due to the initial condition where qubit and the bath are decoupled. Such overall similarity of pure state to pure state transition is not surprising: with coupling to driving force much stronger than dissipation (which is a prerequisite for ability to control the

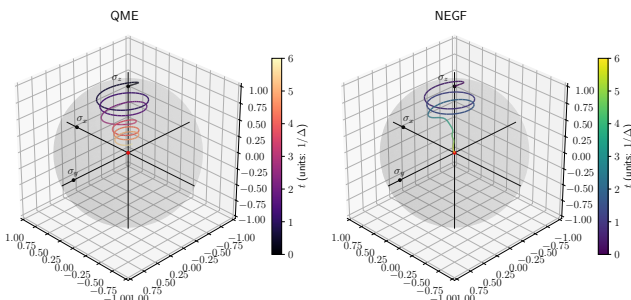
qubit), dissipation almost doesn't play any role in a pure state evolution (note that both trajectories are confined to outer surface of the sphere) while unitary evolution is the same under both QME and NEGF formulations.

## B. Heating

Heating task is the process starting from a pure (cold) state evolving into the maximum entropy state,  $\rho_f = I/2$ . We choose initial (cold) state to be  $\rho_i = (I + \sigma_z)/2$  which corresponds to  $(0, 0, 1)$  vector on the sphere.



(a)



(b)

FIG. 3. (Color online) Heating of the qubit: forced evolution from an arbitrary initial state ( $\rho_i = (I + \sigma_z)/2$ ) to the maximum entropy state ( $\rho_f = I/2$ ). Panel (a) shows (top to bottom) optimal driving force potential, entropy production, entropy of the qubit, and cost function vs. time simulated within QME (dashed line, blue) and NEGF (solid line, orange). Panel (b) shows trajectories of the system within the two formulations.

Figure 3 shows results of simulations performed within

QME and NEGF for  $t_c = 6$ . Contrary to the previous task, evolution involving mixed states demonstrates differences between the results of the two methods. Indeed, change from pure to mixed state is impossible without dissipation. The latter is treated very differently by QME (Markov) and NEGF (non-Markov) formulations. This difference manifests itself in significant deviations of trajectories in the region where the mixed character of the qubit is pronounced, that is deep inside the sphere (see panel b).

Note that NEGF simulation yields non-monotonic entropy change with the possibility to have negative entropy values (see panel a). Both effects are due to dynamics of entanglement formation between system and bath during evolution and are a manifestation of non-negligible system-bath coupling (which is completely missed by the QME formulation).

Note also that for  $t_c = 6$  NEGF is faster in reaching the final state (see bottom graph in panel a). Longer driving ( $t_c = 12$ , not shown) is necessary for the QME to achieve the same goal.

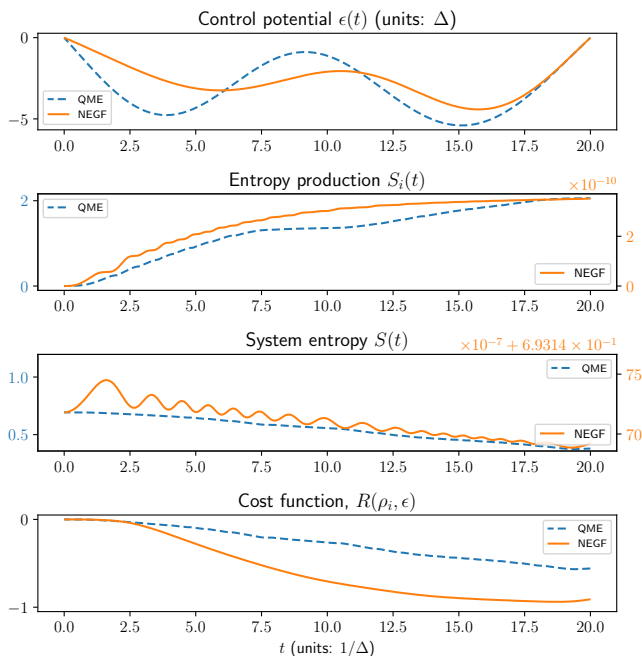
## C. Cooling

Cooling is a process opposite to heating: initial state is the maximum entropy state  $\rho_i = I/2$  which evolves into a pure state  $\rho_f$  where  $|\rho_f| = 1$ .

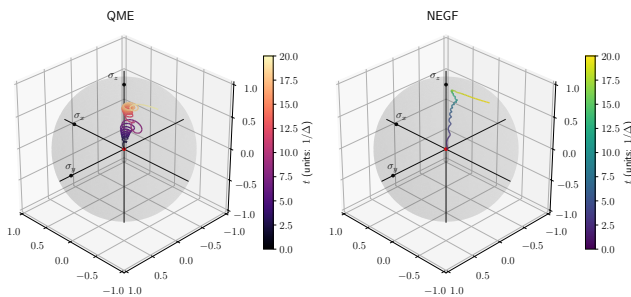
Figure 4 shows results of simulations performed within QME and NEGF for  $t_c = 100$ . As with heating, the evolution involves a mixed state which leads to pronounced differences between QME and NEGF results. As previously, NEGF results demonstrate non-monotonic behavior of system entropy (see panel a) and drastically different trajectory (panel b). Again, NEGF is much more efficient in reaching the final goal (the optimized cost function value is  $-0.64$  for QME and  $-0.91$  for NEGF). Note that simulations with longer driving ( $t_c = 40$ , not shown) also demonstrated the superiority of the NEGF formulation. Moreover, increasing the number of iterations of the optimization cycle from 10 to 100 (not shown) didn't affect the inability of the QME to reach the final goal. The difficulty of the qubit to escape from a low purity state to a high purity state within QME (which is similar to the difficulty of the opposite process, as discussed above in heating task) is due to approximate (adiabatic) treatment of the effect of the driving on system dissipation.

## IV. CONCLUSION

We examine the manipulation of a qubit coupled to a thermal bath using an external driving field. The optimization of the field (the time profile of the driving) aims to achieve a specific outcome (a particular state of the qubit) within a fixed duration of driving. We address three objectives: reset (evolution from an arbitrary



(a)



(b)

FIG. 4. (Color online) Cooling of the qubit: forced evolution from the maximum entropy state ( $\rho_i = I/2$ ) to a pure state ( $\|\rho_f\| = 1$ ). Panel (a) shows (top to bottom) optimal driving force potential, entropy production, entropy of the qubit, and cost function vs. time simulated within QME (dashed line, blue) and NEGF (solid line, orange). Panel (b) shows trajectories of the system within the two formulations.

pure state to a predefined pure state of the qubit), heating (evolution from a pure state to the maximum entropy state,  $\rho_f = I/2$ , of the qubit), and cooling (evolution from the maximum entropy state,  $\rho_f = I/2$ , to a pure state of the qubit).

Typically, studies on optimization in open quantum systems utilize the Redfield/Lindblad quantum master equation (QME) to characterize the system's dynamics. Among the various limitations of this method, the most significant for optimal control is the lack of consideration for the influence of time-dependent driving on the dissipator superoperator (in the standard formulation), or an approximate (adiabatic) approach to account for the effect of driving on dissipation (in the generalized formu-

lation).

We utilize the NEGF, where the impact of driving on dissipation is modeled more accurately, and compare the predictions of the two methods. We find that in evolutions involving pure states (reset), the two formulations yield qualitatively similar results. This is because any optimization task entails a much stronger coupling to the driving field than to the bath. Consequently, the effect of dissipation on dynamics - where the two methods diverge - is minor. Conversely, in evolutions involving mixed states (particularly for transitions between pure and mixed states, as seen in heating and cooling tasks), the two methods produce significantly different results, with the NEGF proving more effective in achieving the desired outcome. This is hardly surprising, as any transition between pure and mixed states necessitates the presence of dissipation.

We note that our simulations were conducted in a parameter regime conducive to employing the Redfield QME. However, the adiabatic approximation used to address the impact of time-dependent driving on dissipation within the method leads to challenges in accurately describing mixed state evolution. This highlights the advantages of non-Markov Green's function techniques and, hopefully, will establish them as a preferred tool for studies on optimization in open quantum systems.

## ACKNOWLEDGMENTS

We thank Ronnie Kosloff and Shimshon Kallush for helpful discussions. This material is based upon work supported by the National Science Foundation under Grant No. CHE-2154323.

## Appendix A: Derivation of Eq.(7)

Derivation of the time-dependent QME (7) follows standard procedure for the Redfield QME<sup>60</sup> with the modification accounting for time-dependence of the driving field on dissipator as is described in Ref. 45.

Specifically, we start from the Redfield equation

$$\frac{d}{dt} \hat{\rho}_S(t) = - \int_0^\infty ds \text{Tr}_B \left\{ \left[ \hat{H}^{SB}(t), \left[ \hat{H}^{SB}(t-s), \hat{\rho}_S(t) \otimes \hat{\rho}_B^{eq} \right] \right] \right\} \quad (\text{A1})$$

Here, tilde indicates interaction picture,  $\hat{\rho}_S(t)$  is the reduced density matrix of the qubit, and  $\hat{\rho}_B^{eq}$  is the equilibrium density operator of the thermal bath.  $\text{Tr}_B \{ \dots \}$  is trace over the bath degrees of freedom.

System-bath coupling (4) in interaction picture is

$$\hat{H}^{SB}(t) \equiv \hat{U}_S^\dagger(t, 0) \frac{i}{2} (\hat{d}_2^\dagger \hat{d}_1 - \hat{d}_1^\dagger \hat{d}_2) \hat{U}_S(t, 0) \otimes \hat{U}_B^\dagger(t, 0) \hat{B} \hat{U}_B(t, 0) \quad (\text{A2})$$

where  $\hat{U}_S(t, 0)$  is the system free evolution operator which satisfies

$$\frac{\partial}{\partial t} \hat{U}_S(t, 0) = -i\hat{H}^S(t) \hat{U}_S(t, 0), \quad (\text{A3})$$

$\hat{B} \equiv \sum_{\alpha} g_{\alpha} (\hat{a}_{\alpha} + \hat{a}_{\alpha}^{\dagger})$ , and  $\hat{U}_B(t, 0)$  describes evolution of free bath which is assumed to be in thermal equilibrium.

Solving numerically free evolution (A3) one can introduce instantaneous eigenproblem for the operator  $\hat{U}_S(t, 0)$

$$\hat{U}_S(t, 0)|S(t)\rangle = e^{-iu_S(t)}|S(t)\rangle \quad (\text{A4})$$

Eigenvectors are used to define instantaneous jump operators

$$\hat{F}_{S_1 S_2}(t) \equiv |S_1(t)\rangle\langle S_2(t)| \quad (\text{A5})$$

which evolve as

$$\begin{aligned} \hat{U}_S^{\dagger}(t, 0)\hat{F}_{S_1 S_2}(t)\hat{U}_S(t, 0) &= e^{i[u_{S_1}(t)-u_{S_2}(t)]}\hat{F}_{S_1 S_2}(t) \\ &\equiv e^{-i\theta_{S_1 S_2}(t)}\hat{F}_{S_1 S_2}(t) \end{aligned} \quad (\text{A6})$$

These jump operators can be used to represent free evolution of any operator acting on system degrees of freedom only. In particular,

$$\begin{aligned} \hat{U}_S^{\dagger}(t, 0) \frac{i}{2} (\hat{d}_2^{\dagger}\hat{d}_1 - \hat{d}_1^{\dagger}\hat{d}_2) \hat{U}_S(t, 0) \\ = \sum_m \xi_m(t) e^{-i\theta_m(t)} \hat{F}_m(t) \end{aligned} \quad (\text{A7})$$

where  $m \equiv (S_1, S_2)$  indicates transition between states of the system and  $\xi_m(t)$  are coefficients of expansion.

Using (A7) in (A1) leads to

$$\begin{aligned} \frac{d}{dt} \hat{\rho}_S(t) &= \sum_{m, m'} \int_0^{\infty} ds \xi_m^*(t) \xi_{m'}(t-s) e^{i[\theta_m(t)-\theta_{m'}(t-s)]} \\ &\times [\hat{F}_{m'}(t-s)\hat{\rho}_S(t)\hat{F}_m^{\dagger}(t) - \hat{F}_m^{\dagger}(t)\hat{F}_{m'}(t-s)\hat{\rho}_S(t)] \\ &\times \left\langle \hat{B}(t) \hat{B}(t-s) \right\rangle_{eq} + \text{H.c.} \end{aligned} \quad (\text{A8})$$

where we used Hermitian property of  $\hat{s}_y$ ,  $\hat{B}$ , Hamiltonian, and density operator, and where

$$\left\langle \hat{B}(t) \hat{B}(t-s) \right\rangle_{eq} \equiv \text{Tr}_B \left\{ \hat{B}(t) \hat{B}(t-s) \hat{\rho}_B^{eq} \right\} \quad (\text{A9})$$

Standard derivation of the Redfield QME implies infinitely fast bath, this allows to approximate

$$\xi_{m'}(t-s) \approx \xi_{m'}(t) \quad \text{and} \quad \hat{F}_{m'}(t-s) \approx \hat{F}_{m'}(t) \quad (\text{A10})$$

Expanding phase factor in (A8) to linear term in time and employing rotating wave approximation,

$$\theta_m(t) - \theta_{m'}(t-s) \approx \delta_{m, m'} \omega_m s, \quad (\text{A11})$$

leads to

$$\begin{aligned} \frac{d}{dt} \hat{\rho}_S(t) &= \\ \sum_m \Gamma_m(t) [\hat{F}_m(t)\hat{\rho}_S(t)\hat{F}_m^{\dagger}(t) - \hat{F}_m^{\dagger}(t)\hat{F}_m(t)\hat{\rho}_S(t)] &+ \text{H.c.} \end{aligned} \quad (\text{A12})$$

where

$$\Gamma_m(t) \equiv |\xi_m(t)|^2 \int_0^{\infty} ds e^{i\omega_m s} \left\langle \hat{B}(s) \hat{B}(0) \right\rangle_{eq} \quad (\text{A13})$$

Expression (A12) is Eq.(7).

## Appendix B: Qubit self-energy due to coupling to thermal bath

It is convenient to express system-bath coupling, Eq.(4) in a more general form

$$\hat{H}^{SB} = \sum_{i,j} v_{ij} d_i^{\dagger} d_j \sum_{\alpha} g_{\alpha} (\hat{a}_{\alpha} + \hat{a}_{\alpha}^{\dagger}) \quad (\text{B1})$$

where  $v_{ij} = \frac{i}{2}(\delta_{i,2}\delta_{j,1} - \delta_{i,1}\delta_{j,2})$ . The coupling is considered to be a perturbation. Below, it is taken into account employing diagrammatic expansion.

Rewriting expression for the single-particle Green's function, Eq.(8), in the interaction picture,

$$G_{ij}(\tau_1, \tau_2) = -i \left\langle T_c \hat{d}_i(\tau_1) \hat{d}_j^{\dagger}(\tau_2) e^{-i \int_c d\tau \hat{H}^{SB}(\tau)} \right\rangle, \quad (\text{B2})$$

expanding evolution operator up to second order in  $\hat{H}^{SB}$ , applying the Wick's theorem, and dressing the diagrams yields the Dyson equation - integral form of the Kadanoff-Baym equation (10)

$$\begin{aligned} G_{ij}(\tau_1, \tau_2) &= G_{ij}^{(0)}(\tau_1, \tau_2) \\ &+ \sum_{l,m} \int_c d\tau \int_c d\tau' G_{il}^{(0)}(\tau_1, \tau) \Sigma_{lm}(\tau, \tau') G_{mj}(\tau', \tau_2) \end{aligned} \quad (\text{B3})$$

where  $G^{(0)}$  is the single-particle Green's function in the absence of of the system-bath coupling and  $\Sigma$  is self-energy due to the coupling. Explicit expression of the self-energy within the second order expansion (the Hartree-Fock approximation) is

$$\Sigma_{lm}(\tau, \tau') = \underbrace{\Sigma_{lm}^H(\tau, \tau')}_{\text{Hartree}} + \underbrace{\Sigma_{lm}^F(\tau, \tau')}_{\text{Fock}} \quad (\text{B4})$$

$$\Sigma_{lm}^H(\tau, \tau') = -i\delta(\tau, \tau') \sum_{m'l'} \int_c d\tau'' v_{lm} v_{l'm'} \quad (\text{B5})$$

$$\times G_{m'l'}(\tau'', \tau''_+) [\sigma(\tau'', \tau) + \sigma(\tau, \tau'')] ]$$

$$\Sigma_{lm}^F(\tau, \tau') = i \sum_{m'l'} v_{lm'} v_{l'm} \quad (\text{B6})$$

$$\times G_{m'l'}(\tau, \tau') [\sigma(\tau', \tau) + \sigma(\tau, \tau')] ]$$

where

$$\sigma(\tau, \tau') = -i \sum_{\alpha} g_{\alpha}^2 \langle T_c \hat{a}_{\alpha}(\tau) \hat{a}_{\alpha}^{\dagger}(\tau') \rangle_0 \quad (\text{B7})$$

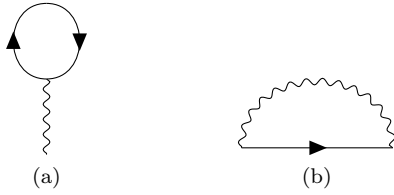


FIG. 5. Feynman diagrams of the self-energy (B4). Shown are (a) Hartree  $\Sigma^H$ , Eq.(B5), and (b) Fock  $\Sigma^F$ , Eq.(B6), contributions.

Here,  $\langle \dots \rangle_0$  indicates free evolution of the bath.

In simulations, we'll need lesser and greater projections of (B7). To obtain those we start from energy domain where

$$\begin{aligned}\sigma^<(\omega) &= -i\gamma(\omega)N(\omega) \\ \sigma^>(\omega) &= -i\gamma(\omega)[N(\omega) + 1]\end{aligned}\quad (\text{B8})$$

and employ FFT. In (B8)

$$\gamma(\omega) = \gamma_0 \left( \frac{\omega}{\omega_c} \right)^2 e^{2(1-\frac{\omega}{\omega_c})} \quad (\text{B9})$$

$$N(\omega) = \frac{1}{e^{\beta\omega} - 1} \quad (\text{B10})$$

are the dissipation rate and Bose-Einstein thermal distribution.

We note that because thermal bath (B8)-(B10) does not support zero frequency modes, only Fock self-energy, Eq.(B6), will contribute.

### Appendix C: NEGF expressions for the heat flux and entropy production rate

Here we derive expressions for heat flux and entropy production rate of a qubit coupled to thermal bath.

We start from considering the particle (phonon) flux on the system-bath interface. The flux is defined as minus rate of change of population in the bath

$$I_B(t) = -\frac{d}{dt} \sum_{\alpha} \langle \hat{a}_{\alpha}^{\dagger}(t) \hat{a}_{\alpha}(t) \rangle \quad (\text{C1})$$

For the Hamiltonian (1)-(4) it can be expressed in terms of mixed Green's function

$$I_B(t) = 2 \text{Re} \left[ \sum_{\alpha} g_{\alpha} G_{\alpha S}^<(t, t) \right] \quad (\text{C2})$$

where the Green's function is lesser projection of

$$G_{\alpha S}(\tau_1, \tau_2) \equiv -i \langle T_c \hat{a}_{\alpha}(\tau_1) \hat{S}^{\dagger}(\tau_2) \rangle \quad (\text{C3})$$

Here,

$$\hat{S} \equiv \frac{i}{2} (\hat{d}_2^{\dagger} \hat{d}_1 - \hat{d}_1^{\dagger} \hat{d}_2) \quad (\text{C4})$$

Using the Dyson equation, mixed Green's function is expressed in terms of free bath and system evolutions as

$$G_{\alpha S}(\tau_1, \tau_2) = \int_c d\tau F_{\alpha}^{(0)}(\tau_1, \tau) g_{\alpha} G_{SS}(\tau, \tau_2) \quad (\text{C5})$$

where

$$F_{\alpha}^{(0)}(\tau_1, \tau_2) = -i \langle T_c \hat{a}_{\alpha}(\tau_1) \hat{a}_{\alpha}^{\dagger}(\tau_2) \rangle_0 \quad (\text{C6})$$

$$G_{SS}(\tau_1, \tau_2) = -i \langle T_c \hat{S}(\tau_1) \hat{S}^{\dagger}(\tau_2) \rangle \quad (\text{C7})$$

are Green's functions describing evolution of free bath phonon and full system excitation, respectively.

Substituting lesser projection of (C5) into (C2) leads to

$$\begin{aligned}I_B(t) &= -2 \text{Re} \int_0^t dt' \int \frac{d\omega}{2\pi} e^{-i\omega(t-t')} \\ &\quad \times [\sigma^<(\omega) G_{SS}^>(t', t) - \sigma^>(\omega) G_{SS}^<(t', t)] \\ &\equiv \int \frac{d\omega}{2\pi} i_B(t, \omega)\end{aligned}\quad (\text{C8})$$

Here,  $i_B(t, \omega)$  is the energy resolved particle (phonon) flux and  $\sigma^{\lessgtr}$  is Fourier transform of the lesser/greater projection of

$$\sigma(\tau_1, \tau_2) \equiv \sum_{\alpha} g_{\alpha}^2 F_{\alpha}^{(0)}(\tau_1, \tau_2) \quad (\text{C10})$$

Explicit expressions of the projections are given in Eq.(B8).

In terms of energy resolved particle flux (C9), heat flux (which for the thermal bath is equivalent to energy flux) is

$$\dot{Q}_B(t) = \int_0^{\infty} \frac{d\omega}{2\pi} \omega i_B(t, \omega) \quad (\text{C11})$$

To derive expression for entropy production, we express particle flux (C8) as difference between incoming thermal and outgoing non-thermal fluxes. In writing this expression we take into account that in 1D velocity exactly cancels with density of states<sup>61</sup>. Thus,

$$I_B(t) = \int \frac{d\omega}{2\pi} [\phi^{in}(\omega) - \phi^{out}(t, \omega)] \quad (\text{C12})$$

Because expression for thermal population is known,

$$\phi^{in}(\omega) = N(\omega), \quad (\text{C13})$$

Eqs. (C9) and (C12) yield expression for outgoing non-thermal flux

$$\phi^{out}(t, \omega) = \phi^{in}(\omega) - i_B(t, \omega) \quad (\text{C14})$$

Rate of entropy change is introduced as a difference between incoming and outgoing entropy fluxes

$$\frac{dS}{dt} = \int \frac{d\omega}{2\pi} (\sigma[\phi^{in}(\omega)] - \sigma[\phi^{out}(t, \omega)]) \quad (\text{C15})$$

where

$$\sigma[\phi] \equiv -\phi \ln \phi - (1 - \phi) \ln(1 - \phi) \quad (\text{C16})$$

is the von Neumann expression for entropy in the bath. Finally, using (C11) and (C15) in (15) yields expression

for entropy production<sup>59</sup>

$$\begin{aligned} \dot{S}_i(t) = \int_0^\infty \frac{d\omega}{2\pi} & \left\{ \phi^{out}(t, \omega) [\ln \phi^{out}(t, \omega) - \ln \phi^{in}(\omega)] \right. \\ & \left. - (1 + \phi^{out}(t, \omega)) [\ln(1 + \phi^{out}(t, \omega)) - \ln(1 + \phi^{in}(\omega))] \right\} \end{aligned} \quad (\text{C17})$$

Note that consideration above is done in the diagonal approximation. General formulation can be found in Ref. 59.

- 
- \* migalperin@ucsd.edu
- <sup>1</sup> O. Gühne, E. Haapasalo, T. Kraft, J.-P. Pellonpää, and R. Uola, Colloquium: Incompatible measurements in quantum information science, *Rev. Mod. Phys.* **95**, 011003 (2023).
  - <sup>2</sup> G. Tóth and I. Apellaniz, Quantum metrology from a quantum information science perspective, *J. Phys. A* **47**, 424006 (2014).
  - <sup>3</sup> G. Adesso, T. R. Bromley, and M. Cianciaruso, Measures and applications of quantum correlations, *J. Phys. A* **49**, 473001 (2016).
  - <sup>4</sup> M.-L. Hu, X. Hu, J. Wang, Y. Peng, Y.-R. Zhang, and H. Fan, Quantum coherence and geometric quantum discord, *Phys. Rep.* **762-764**, 1 (2018).
  - <sup>5</sup> R. Uola, A. C. Costa, H. C. Nguyen, and O. Gühne, Quantum steering, *Rev. Mod. Phys.* **92**, 015001 (2020).
  - <sup>6</sup> E. Chitambar and G. Gour, Quantum resource theories, *Rev. Mod. Phys.* **91**, 025001 (2019).
  - <sup>7</sup> J. Goold, M. Huber, A. Riera, L. d. Rio, and P. Skrzypczyk, The role of quantum information in thermodynamics—a topical review, *J. Phys. A* **49**, 143001 (2016).
  - <sup>8</sup> S. Vinjanampathy and J. Anders, Quantum thermodynamics, *Contemp. Phys.* **57**, 545 (2016).
  - <sup>9</sup> R. Kosloff, Quantum thermodynamics and open-systems modeling, *J. Chem. Phys.* **150**, 204105 (2019).
  - <sup>10</sup> J. P. Palao and R. Kosloff, Quantum Computing by an Optimal Control Algorithm for Unitary Transformations, *Phys. Rev. Lett.* **89**, 188301 (2002).
  - <sup>11</sup> S. Kallush and R. Kosloff, Scaling the robustness of the solutions for quantum controllable problems, *Phys. Rev. A* **83**, 063412 (2011).
  - <sup>12</sup> S. J. Glaser, U. Boscain, T. Calarco, C. P. Koch, W. Köckenberger, R. Kosloff, I. Kuprov, B. Luy, S. Schirmer, T. Schulte-Herbrüggen, D. Sugny, and F. K. Wilhelm, Training Schrödinger’s cat: quantum optimal control, *Eur. Phys. J. D* **69**, 279 (2015).
  - <sup>13</sup> S. Deffner and S. Campbell, Quantum speed limits: from Heisenberg’s uncertainty principle to optimal quantum control, *J. Phys. A* **50**, 453001 (2017).
  - <sup>14</sup> M. Bukov, A. G. Day, D. Sels, P. Weinberg, A. Polkovnikov, and P. Mehta, Reinforcement Learning in Different Phases of Quantum Control, *Phys. Rev. X* **8**, 031086 (2018).
  - <sup>15</sup> A. Frisk Kockum, A. Miranowicz, S. De Liberato, S. Savasta, and F. Nori, Ultrastrong coupling between light and matter, *Nat. Rev. Phys.* **1**, 19 (2019).
  - <sup>16</sup> D. Guéry-Odelin, A. Ruschhaupt, A. Kiely, E. Torrontegui, S. Martínez-Garaot, and J. Muga, Shortcuts to adiabaticity: Concepts, methods, and applications, *Rev. Mod. Phys.* **91**, 045001 (2019).
  - <sup>17</sup> C. P. Koch, U. Boscain, T. Calarco, G. Dirr, S. Filipp, S. J. Glaser, R. Kosloff, S. Montangero, T. Schulte-Herbrüggen, D. Sugny, and F. K. Wilhelm, Quantum optimal control in quantum technologies. Strategic report on current status, visions and goals for research in Europe, *EPJ Quantum Technol.* **9**, 1 (2022).
  - <sup>18</sup> A. P. Peirce, M. A. Dahleh, and H. Rabitz, Optimal control of quantum-mechanical systems: Existence, numerical approximation, and applications, *Phys. Rev. A* **37**, 4950 (1988).
  - <sup>19</sup> R. Kosloff, S. A. Rice, P. Gaspard, S. Tersigni, and D. J. Tannor, Wavepacket dancing: Achieving chemical selectivity by shaping light pulses, *Chem. Phys.* **139**, 201 (1989).
  - <sup>20</sup> T. Szakács, B. Amstrup, P. Gross, R. Kosloff, H. Rabitz, and A. Lörincz, Locking a molecular bond: A case study of CsI, *Phys. Rev. A* **50**, 2540 (1994).
  - <sup>21</sup> J. P. Palao and R. Kosloff, Optimal control theory for unitary transformations, *Phys. Rev. A* **68**, 062308 (2003).
  - <sup>22</sup> C. P. Koch, J. P. Palao, R. Kosloff, and F. Masnou-Seeuws, Stabilization of ultracold molecules using optimal control theory, *Phys. Rev. A* **70**, 013402 (2004).
  - <sup>23</sup> J. P. Palao, R. Kosloff, and C. P. Koch, Protecting coherence in optimal control theory: State-dependent constraint approach, *Phys. Rev. A* **77**, 063412 (2008).
  - <sup>24</sup> M. Tomza, M. H. Goerz, M. Musiał, R. Moszynski, and C. P. Koch, Optimized production of ultracold ground-state molecules: Stabilization employing potentials with ion-pair character and strong spin-orbit coupling, *Phys. Rev. A* **86**, 043424 (2012).
  - <sup>25</sup> A. Aroch, S. Kallush, and R. Kosloff, Optimizing the multi-cycle subrotational internal cooling of diatomic molecules, *Phys. Rev. A* **97**, 053405 (2018).
  - <sup>26</sup> I. Schaefer and R. Kosloff, Optimization of high-order harmonic generation by optimal control theory: Ascending a functional landscape in extreme conditions, *Phys. Rev. A* **101**, 023407 (2020).
  - <sup>27</sup> M. Ndong, H. Tal-Ezer, R. Kosloff, and C. P. Koch, A Chebychev propagator for inhomogeneous Schrödinger equations, *J. Chem. Phys.* **130**, 124108 (2009).
  - <sup>28</sup> M. Rossignolo, T. Reisser, A. Marshall, P. Rembold, A. Pagano, P. J. Vetter, R. S. Said, M. M. Müller, F. Motzoi, T. Calarco, F. Jelezko, and S. Montangero, QuOCS: The quantum optimal control suite, *Comput. Phys. Commun.* **291**, 108782 (2023).

- <sup>29</sup> R. Baer and R. Kosloff, Quantum dissipative dynamics of adsorbates near metal surfaces: A surrogate Hamiltonian theory applied to hydrogen on nickel, *J. Chem. Phys.* **106**, 8862 (1997).
- <sup>30</sup> D. Gelman and R. Kosloff, Minimizing broadband excitation under dissipative conditions, *J. Chem. Phys.* **123**, 234506 (2005).
- <sup>31</sup> E. Asplund and T. Klüner, Optimal Control of Open Quantum Systems Applied to the Photochemistry of Surfaces, *Phys. Rev. Lett.* **106**, 140404 (2011).
- <sup>32</sup> E. Asplund and T. Klüner, Optimal control of open quantum systems: A combined surrogate Hamiltonian optimal control theory approach applied to photochemistry on surfaces, *J. Chem. Phys.* **136**, 124118 (2012).
- <sup>33</sup> M. Abdelhafez, D. I. Schuster, and J. Koch, Gradient-based optimal control of open quantum systems using quantum trajectories and automatic differentiation, *Phys. Rev. A* **99**, 052327 (2019).
- <sup>34</sup> A. Bartana, R. Kosloff, and D. J. Tannor, Laser cooling of molecular internal degrees of freedom by a series of shaped pulses, *J. Chem. Phys.* **99**, 196 (1993).
- <sup>35</sup> H. Tang, R. Kosloff, and S. A. Rice, A generalized approach to the control of the evolution of a molecular system, *J. Chem. Phys.* **104**, 5457 (1996).
- <sup>36</sup> D. J. Tannor, R. Kosloff, and A. Bartana, Laser cooling of internal degrees of freedom of molecules by dynamically trapped states, *Faraday Discussions* **113**, 365 (1999).
- <sup>37</sup> Y. Ohtsuki, W. Zhu, and H. Rabitz, Monotonically convergent algorithm for quantum optimal control with dissipation, *J. Chem. Phys.* **110**, 9825 (1999).
- <sup>38</sup> A. Bartana, R. Kosloff, and D. J. Tannor, Laser cooling of molecules by dynamically trapped states, *Chem. Phys.* **267**, 195 (2001).
- <sup>39</sup> R. Xu, Y. Yan, Y. Ohtsuki, Y. Fujimura, and H. Rabitz, Optimal control of quantum non-Markovian dissipation: Reduced Liouville-space theory, *J. Chem. Phys.* **120**, 6600 (2004).
- <sup>40</sup> G. Katz, M. A. Ratner, and R. Kosloff, Decoherence Control by Tracking a Hamiltonian Reference Molecule, *Phys. Rev. Lett.* **98**, 203006 (2007).
- <sup>41</sup> D. Basilewitsch, R. Schmidt, D. Sugny, S. Maniscalco, and C. P. Koch, Beating the limits with initial correlations, *New J. Phys.* **19**, 113042 (2017).
- <sup>42</sup> D. Basilewitsch, C. P. Koch, and D. M. Reich, Quantum Optimal Control for Mixed State Squeezing in Cavity Optomechanics, *Adv. Quantum Technol.* **2**, 1800110 (2019).
- <sup>43</sup> A. Aroch, R. Kosloff, and S. Kallush, Employing typicality in optimal control theory: Addressing large Hilbert spaces, *Phys. Rev. A* **107**, 022603 (2023).
- <sup>44</sup> R. Dann and R. Kosloff, Quantum thermo-dynamical construction for driven open quantum systems, *Quantum* **5**, 590 (2021).
- <sup>45</sup> S. Kallush, R. Dann, and R. Kosloff, Controlling the uncontrollable: Quantum control of open-system dynamics, *Sci. Adv.* **8**, eadd0828 (2022).
- <sup>46</sup> M. Lostaglio, An introductory review of the resource theory approach to thermodynamics, *Rep. Prog. Phys.* **82**, 114001 (2019).
- <sup>47</sup> M. Esposito, M. A. Ochoa, and M. Galperin, Efficiency fluctuations in quantum thermoelectric devices, *Phys. Rev. B* **91**, 115417 (2015).
- <sup>48</sup> Y. Gao and M. Galperin, Simulation of optical response functions in molecular junctions, *J. Chem. Phys.* **144**, 244106 (2016).
- <sup>49</sup> E. Mangaud, R. Puthumpally-Joseph, D. Sugny, C. Meier, O. Atabek, and M. Desouter-Lecomte, Non-Markovianity in the optimal control of an open quantum system described by hierarchical equations of motion, *New J. Phys.* **20**, 043050 (2018).
- <sup>50</sup> A. Erpenbeck, C. Hertlein, C. Schinabeck, and M. Thoss, Extending the hierarchical quantum master equation approach to low temperatures and realistic band structures, *J. Chem. Phys.* **149**, 064106 (2018).
- <sup>51</sup> G. Cohen and M. Galperin, Green's function methods for single molecule junctions, *J. Chem. Phys.* **152**, 090901 (2020).
- <sup>52</sup> M. J. Hyrkäs, D. Karlsson, and R. van Leeuwen, Cutting rules and positivity in finite temperature many-body theory, *J. Phys. A* **55**, 335301 (2022).
- <sup>53</sup> R. Dann, A. Levy, and R. Kosloff, Time-dependent Markovian quantum master equation, *Phys. Rev. A* **98**, 052129 (2018).
- <sup>54</sup> W. H. Press, S. A. Teukolsky, W. T. Vetterling, and B. P. Flannery, *Numerical Recipes in C. The Art of Scientific Computing*. (Cambridge University Press, 1997).
- <sup>55</sup> A. Stan, N. E. Dahlen, and R. van Leeuwen, Time propagation of the Kadanoff–Baym equations for inhomogeneous systems, *J. Chem. Phys.* **130**, 224101 (2009).
- <sup>56</sup> M. Frigo and S. G. Johnson, The design and implementation of fftw3, *Proc. IEEE* **93**, 216 (2005).
- <sup>57</sup> R. Storn and K. Price, Differential Evolution – A Simple and Efficient Heuristic for global Optimization over Continuous Spaces, *J. Glob. Optim.* **11**, 341 (1997).
- <sup>58</sup> K. Ptaszyński and M. Esposito, Thermodynamics of Quantum Information Flows, *Phys. Rev. Lett.* **122**, 150603 (2019).
- <sup>59</sup> J. Zhou, A. Li, and M. Galperin, Quantum thermodynamics: Inside-outside perspective, *Phys. Rev. B* **109**, 085408 (2024).
- <sup>60</sup> H.-P. Breuer and F. Petruccione, *The Theory of Open Quantum Systems* (Oxford University Press, Oxford New York, 2003).
- <sup>61</sup> M. Büttiker, Scattering theory of current and intensity noise correlations in conductors and wave guides, *Phys. Rev. B* **46**, 12485 (1992).